Novel Coplanar-Waveguide Bandpass Filters Using Loaded Air-Bridge Enhanced Capacitors and Broadside-Coupled Transition Structures for Wideband Spurious Suppression

Shih-Cheng Lin, Tsung-Nan Kuo, Yo-Shen Lin, *Member, IEEE*, and Chun Hsiung Chen, *Fellow, IEEE*

***Abstract*—Novel inline coplanar-waveguide (CPW) bandpass filters composed of quarter-wavelength stepped-impedance resonators are proposed, using loaded air-bridge enhanced capacitors and broadside-coupled microstrip-to-CPW transition structures for both wideband spurious suppression and size miniaturization. First, by suitably designing the loaded capacitor implemented by enhancing the air bridges printed over the CPW structure and the resonator parameters, the lower order spurious passbands of the proposed filter may effectively be suppressed. Next, by adopting the broadside-coupled microstrip-to-CPW transitions as the fed structures to provide required input and output coupling capacitances and high attenuation level in the upper stopband, the filter with suppressed higher order spurious responses may be achieved. In this study, two second- and fourth-order inline bandpass filters with wide rejection band are implemented and thoughtfully examined. Specifically, the proposed second-order filter has its stopband extended up to $13.3f_0$, where f_0 stands for the passband center frequency, and the fourth-order filter even possesses better stopband up to $19.04f_0$ with a satisfactory rejection greater than 30 dB.**

***Index Terms*—Air bridge, bandpass filter, coplanar waveguide (CPW), microstrip, quarter-wavelength resonator, spurious suppression, stepped-impedance resonator (SIR).**

I. Introduction

COPLANAR WAVEGUIDE (CPW) as one type of popular guided structures [1] has received much attention in the field of bandpass-filter design. Comparing with other planar transmission-line configurations, such as microstrip lines, the CPW permits easier integration of both series and shunt components since its grounds are located on the same surface as the signal line. It also possesses the features such as low dispersion, easy fabrication of short-circuited elements, and insensitivity to the substrate thickness, etc. With such advantages, the CPW turns into an admirable candidate for microwave filter implementation.

Manuscript received March 1, 2006; revised May 2, 2006. This work was supported by the National Science Council of Taiwan under Grant NSC 94-2752-E-002-001-PAE, Grant NSC 94-2219-E-002-008, and Grant NSC 94-2213-E-002-055.

S.-C. Lin, T.-N. Kuo, and C. H. Chen are with the Department of Electrical Engineering and Graduate Institute of Communication Engineering, National Taiwan University, Taipei 106, Taiwan, R.O.C. (e-mail: chchen@ew.ee.ntu.edu.tw).

Y.-S. Lin is with the Department of Electrical Engineering, National Central University, Chungli 320, Taiwan, R.O.C.

Digital Object Identifier 10.1109/TMTT.2006.879175

Over the past few years, a considerable amount of studies have been made on the development of CPW bandpass filters. Capacitively end-coupled half-wavelength ($\lambda/2$) resonator filters built in the CPW by excavating gaps in the center conductor were investigated in [2]. To circumvent the high radiation loss produced from the gaps, inductively direct-coupled bandpass filters [3], [4] were demonstrated by means of patterning a thin strip across the center conductor to join the grounds. The CPW $\lambda/2$ filters with attenuation poles for improved skirt selectivity were proposed both in [5] by using tapped feeds for input/output and interstage couplings and in [6] by rearranging the meander-line interval and shape to introduce cross coupling. Since these filters are principally based on $\lambda/2$ uniform-impedance resonators, their spurious passbands are observed around multiples of the passband center frequency nf_0 $(n = 2, 3, \ldots)$.

For the purposes of size miniaturization and pushing the first spurious passband higher, quarter-wavelength ($\lambda/4$) resonators are adopted in CPW filter design. The tapped-feed combline-type bandpass filters using the CPW resonators were presented in 1995 [7]. Distinct from the conventional combline-type configuration, the CPW $\lambda/4$ resonators with two ends driven by series-capacitive and shunt-inductive coupling elements [8] were designed into hairpin shapes to implement a miniaturized end-coupled filter owning multiple passes. Furthermore, originated from the $\lambda/4$ transmission-line stepped-impedance resonators (SIRs), which are composed of transmission lines (TLs) with different characteristic impedances [9], the $\lambda/4$ SIR inline CPW filter was proposed in [10] on the basis of a conventional filter designed with impedance inverters. As regards the spurious passbands, the filters consisting of $\lambda/4$ resonators have the higher order resonances occurring around $(2n-1)f_0$ $(n = 2, 3, \ldots)$, instead of nf_0 $(n = 2, 3, \ldots)$ for the ones made of $\lambda/2$ resonators.

Since the filters composed of distributed elements inevitably come into existence of unwanted spurious responses in the upper frequency band, which may degrade the filter performance in rejecting the out-of-band interference, numerous attempts have been made using various techniques [11]–[14] to break away from those annoying spurious passbands. By means of proper tappings at both input and output resonators, two independent notches can be created at specified frequencies, thereby neutralizing the spurious passbands [11]. Only those bandpass filters with tapped input/output feeds may take advan-

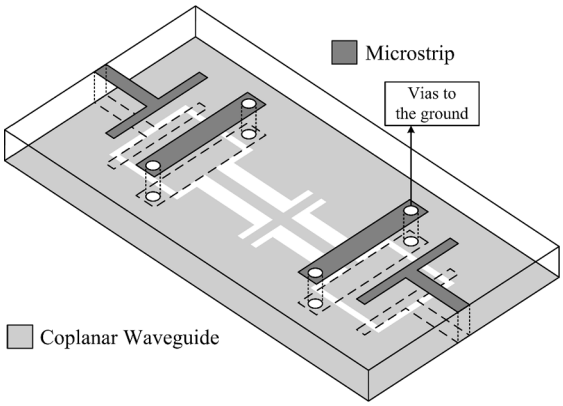

Fig. 1. Three-dimensional physical layout of the proposed second-order inline CPW bandpass filter loaded by air-bridge enhanced capacitors and fed by microstrip-to-CPW transition structures for wideband rejection.

tage of these notches to suppress the spurious responses. For the sake of removing the second harmonic response $(2f_0)$ of conventional microstrip parallel coupled-line filters, omnigenous notions to equalize the even- and odd-mode velocities were reported [12]–[14] such as perturbing the shapes of couple-line sections, employing the suspended coupled microstrips on a substrate with a proper suspension height, etc. By using various dissimilar $\lambda/4$ SIRs, wide-stopband filters may be accomplished [15]. However, the utilization of dissimilar resonators for spurious suppression demands long tuning period and destructs the symmetry of the whole filter structure.

Up to now, the focus of the published literature was mainly on the improvement of the out-of-band attenuation performance of microstrip-type filters. Little attention has been drawn to the spurious-suppression methods suitable for filters of CPW type [16], [17], especially to those adequate for the inline CPW bandpass filter. The particular pattern of via-holes was used in the double-surface CPW filter [16] to reduce the spurious responses. Another four-pole bandpass filter was introduced in [17] using the two asymmetric parallel-coupled CPW stages at the input/output terminated ends to generate the two separated transmission zeros for cancelling the harmonic passband occurring at $3f_0$.

As mentioned above, very few published documents were reported to achieve wide rejection band and effective suppression of the spurious passbands, especially for the inline CPW bandpass filter design. In this paper, novel inline CPW bandpass filters with very wide rejection band are proposed. The proposed filter configuration is composed of CPW $\lambda/4$ SIRs, which are loaded by the air-bridge enhanced capacitors for lower order spurious suppression, as well as size reduction, and are coupled to the input/output ports through the microstrip-to-CPW transition structures for higher order spurious attenuation. Fig. 1 shows one demonstration of a proposed second-order inline CPW filter for wide stopband performance. The loaded lumped-element capacitors are implemented by means of enhancing the air-bridge strips printed over the CPW structure. By properly adjusting the loaded capacitors, the odd-number spurious passbands of proposed filters may essentially be destructed. Moreover, the transmission zero

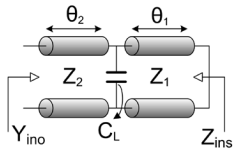

Fig. 2. Equivalent transmission-line model of the proposed $\lambda/4$ SIR loaded by a lumped-element capacitor ($Y_2 = 1/Z_2, Y_1 = 1/Z_1, R_z = Z_2/Z_1 = Y_1/Y_2$).

inherently associated with the air-bridge enhanced capacitors may suitably be allocated to cancel the second spurious passband, thereby effectively suppressing the lower order spurious passbands. In addition, by adopting the broadside-coupled microstrip-to-CPW transitions as the input/output fed structures so as to provide required input/output capacitive couplings at the passband and also to give a high attenuation level in the upper stopband, the remaining unsuppressed higher order spurious passbands of proposed filter may effectively be attenuated. In this study, the concepts of spurious destruction, lower order spurious cancellation, and higher order spurious attenuation are demonstrated by the full-wave simulation of a proposed second-order filter. By making full use of the above-mentioned spurious-suppression mechanisms, second- and fourth-order inline CPW bandpass filters are implemented with the stopbands extended up to $13.3f_0$ and $19.04f_0$.

II. SIRs Loaded by Air-Bridge Enhanced Capacitors

A. Resonance Condition

The equivalent transmission-line model of the proposed $\lambda/4$ SIR loaded by a lumped-element capacitor is shown in Fig. 2. The resonator is composed of two transmission-line sections with unequal characteristic impedances. The section with open-circuited termination has a characteristic impedance Z_2 and electrical length θ_2, while the section with short-circuited termination owns characteristic impedance Z_1 and electrical length θ_1. A lumped-element capacitor with capacitance C_L is attached between the two sections. For this proposed resonator, the input admittance Y_{ino} seen from the open-end side and the input impedance Z_{ins} seen form the short-end side are simply given by

$$Y_{\text{ino}} = Y_2 \frac{j(B_L - Y_1 \cot\theta_1) + jY_2 \tan\theta_2}{Y_2 - (B_L - Y_1 \cot\theta_1)\tan\theta_2} \tag{1}$$

$$Z_{\text{ins}} = \frac{Y_1 - B_L \tan\theta_1 - Y_2 \tan\theta_1 \tan\theta_2}{jY_1(B_L + Y_2 \tan\theta_2 + Y_1 \tan\theta_1)} \tag{2}$$

where $B_L = \omega C_L$ denotes the susceptance of the loaded capacitor. The proposed resonator (Fig. 2) exhibits parallel or series resonances when $Y_{\text{ino}} = 0$ or $Z_{\text{ins}} = 0$, both leading to the resonance condition

$$R_z - \tan\theta_1 \cdot \tan\theta_2 - B_L/Y_2 \tan\theta_1 = 0 \tag{3}$$

where $R_z = Z_2/Z_1 = Y_1/Y_2$ represents the impedance ratio between low- and high-impedance sections. With the aid of the

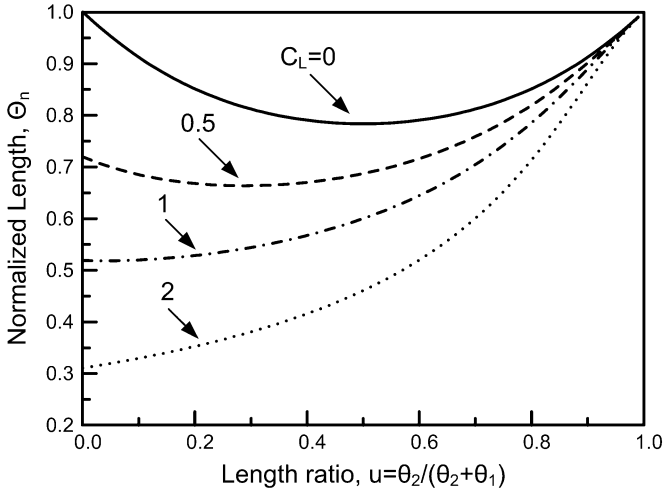

Fig. 3. Normalized length versus the length ratio with C_L (in picofarads) as parameters.

simple (3), the fundamental and higher order resonant frequencies may easily be calculated. Note that these results reduce to those in [9] when $C_L = 0$, as expected.

To demonstrate the effect of the loaded capacitor, Fig. 3 shows the relationship between the length ratio $u[= \theta_2/(\theta_1 + \theta_2)]$ and the normalized resonator length $\Theta_n[=2(\theta_1 + \theta_2)/\pi]$ for $R_z = 0.5$. Here, the value of Z_2 has been fixed to be 50 Ω and the center frequency (f_0) is set to be 1.5 GHz to facilitate the calculation. One can easily observe from Fig. 3 that the larger the capacitance, the more evident the capacitor reduces the normalized length. Equivalently, the size of the proposed resonator may be reduced by simply increasing the loaded capacitor without requiring large impedance difference between low- and high-impedance sections. It is known that a very low impedance ratio sometimes is not achievable under the fabrication process limit since low R_z requires extremely wide or narrow metal-strip width. Wide metal-strip width may cause transverse resonance, while narrow metal-strip width may increase the conductor loss. With the aid of our proposed resonator, the requirement of enforcing low R_z for resonator miniaturization may be prevented.

B. Physical Realization and Model Extraction

Bond wires or air bridges are common in CPW design for suppressing the unwanted modes such as the slot-line mode. Thin wires are usually introduced to keep original circuits unperturbed. The loaded capacitor for the proposed resonator can simply be implemented by enhancing the conventional air bridges. The three-dimensional physical realization and the top-/bottom-plane layouts of the proposed SIR loaded by air-bridge enhanced capacitor are shown in Fig. 4(a) and (b). The physical widths W_1 and W_2 are determined by the impedance ratio of the resonator, while the lengths D_1 and D_2 are governed by the length ratio. By employing a metal strip printed over the CPW structure and connecting two ends of the strip to CPW grounds through via-holes, an air-bridge enhanced capacitor can be constructed. The strip not only plays the role of suppressing the unwanted modes, but also serves as

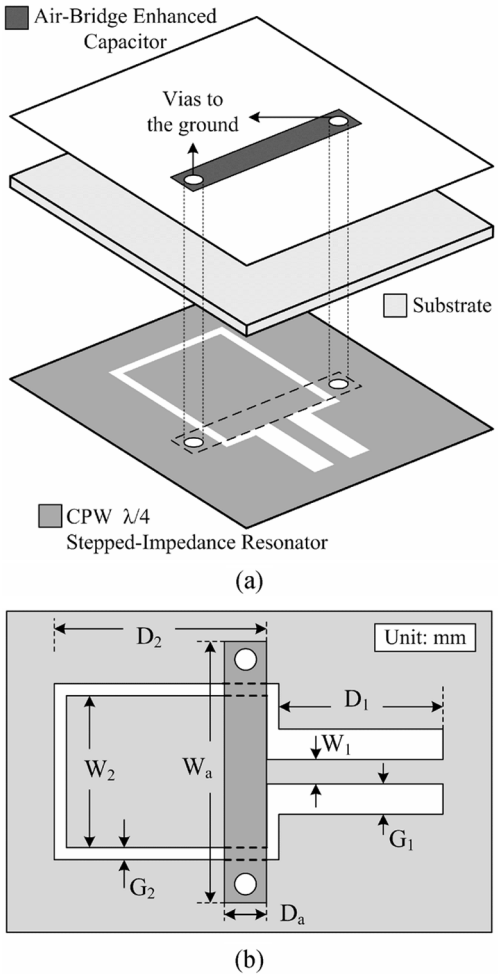

Fig. 4. (a) Three-dimensional physical layout. (b) Top-/bottom-plane layouts of the proposed CPW $\lambda/4$ SIR loaded by air-bridge enhanced capacitor with dimensions labeled $(W_1 = 1.02, G_1 = 1.27, W_2 = 6.35, G_2 = 0.51, W_a = 11.56, D_a = 1.78)$.

a shunt capacitor across the middle of SIR. As observed from Fig. 4, the region formed by the CPW center conductor and the metal strip of the air-bridge span provides the metal–insulator–metal capacitance. However, due to the fringing effect, step discontinuity, and some parasitic effects, this structure becomes too complicated to be analyzed.

Although the use of via-holes is somewhat of a drawback, industry may build large number of via-holes without adding too much cost and complexity in the modern fabrication process. Alternatively, the use of via-holes provides the advantage that facilitates the designers to extend microwave components from planar structure to three-dimensional topology. Therefore, the occupied size of components may become miniaturized, as expected. In this study, by making good use of via-holes, one may build loaded capacitors in the CPW structure with satisfactory large capacitance.

Actually, the enhanced air-bridge structure behaves capacitive at lower frequency band, but resonates at higher frequency. The lumped-element model shown in Fig. 5(a) may be adopted to characterize this structure by setting two ports at low- and high-impedance lines separately. The inductors L_{t1}, L_{t2}, and capacitors C_{t2} are contributed by discontinuity effects. The

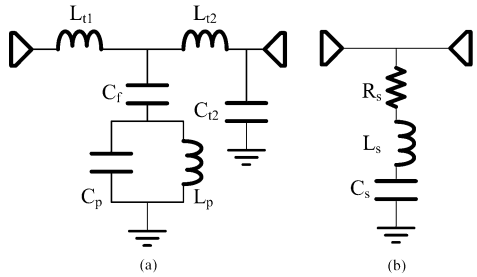

Fig. 5. (a) Lumped-element model. (b) Simplified *RLC* resonator model of the proposed air-bridge enhanced capacitor.

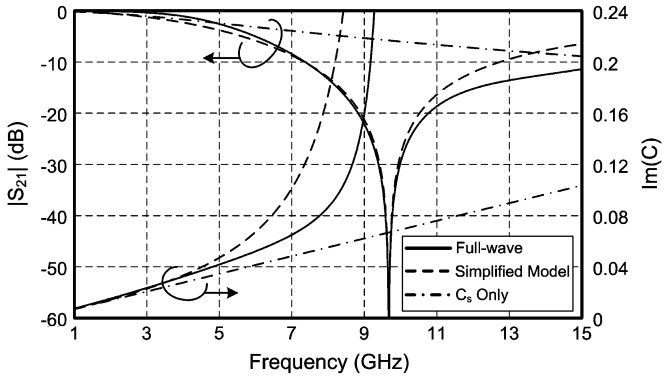

Fig. 6. Comparison of the results, for the structure shown in Fig. 4(a), from full-wave simulation and a simplified model. Here, C represents one of the $ABCD$-matrix parameters of the structure.

kernel portion of the enhanced air bridge is modeled by the coupling capacitor C_f and the *LC* resonant tank (L_p and C_p). Each element value for this model may be extracted from full-wave simulated scattering parameters through optimization. Since the enhanced air bridge behaves like a series resonator, it can approximately be modeled as a series *RLC* resonator, as shown in Fig. 5(b). As a matter of fact, the model in Fig. 5(a) may show better agreement with the real structure, but its application will be restricted. Accordingly, the simplified model [see Fig. 5(b)] is used in the following discussion. In the beginning, the approximate parameters for the simplified series resonator model may be extracted using the equations given in [18]. The relationship between the transmission coefficient and R_s, L_s, and C_s may be expressed as

$$|S_{21}|^2 = \frac{4(1-\omega^2 L_s C_s)^2 + 4R_s^2\omega^2}{4(1-\omega^2 L_s C_s)^2 + \omega^2 C_s^2 (2R_s + Z_0)^2}. \quad (4)$$

From (4), one may evaluate the values of R_s, L_s, and C_s, as given by

$$R_s = \left.\frac{Z_0|S_{21}|}{2(1-|S_{21}|)}\right|_{\omega_{\rm res}} \quad (5a)$$

$$L_s = \frac{\sqrt{a^2(2R_s+Z_0)^2 - 4R_s^2}}{2(\omega_2-\omega_1)\sqrt{1-a^2}}$$

$$C_s = 1/\omega_{\rm res}^2 L_s \quad (5b)$$

where $\omega_{\rm res}$ represents the series resonant frequency, $a = 2|S_{21}|_{\omega_{\rm res}}$, and ω_1 and ω_2 are the frequencies at which $|S_{21}| = a$.

Fig. 6 illustrates the comparison between full-wave simulated and simplified model results including the transmission coefficient and the imaginary part of "C," which is one of the $ABCD$-matrix parameters. The air-bridge enhanced structure is fabricated on a Rogers RO4003 substrate of thickness 0.508 mm, dielectric constant 3.38, metal thickness 17 μm, and loss tangent 0.0027. The diameter of via-holes is 1 mm. The dimensions for the simulated structure are annotated in Fig. 4. The extracted element values of the simplified model are $L_s = 0.246$ nH and $C_s = 1.099$ pF. Note that the responses for full-wave simulation and a simplified model coincide well over a wide frequency range. In the lower frequency band, this simplified model may be reduced to only a capacitor C_s left since the inductor L_s will be of minor significance. Therefore, the equivalent loaded capacitance C_L of this structure approximately equals C_s. The related simulated result of using C_s only is also included in Fig. 6 for comparison.

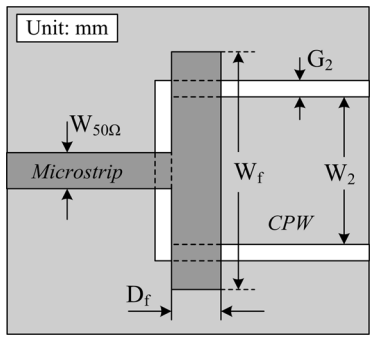

Fig. 7. Top-/bottom-plane layouts of the broadside-coupled microstrip-to-CPW transition for higher order spurious attenuation with W_f to be adjusted. ($W_{50\,\Omega} = 1.12, D_f = 1.1, W_2 = 6.35, G_2 = 0.51$, the substrate thickness $h = 0.508$, the dielectric constant $\varepsilon_r = 3.38$).

III. Broadside-Coupled Microstrip-to-CPW Transition Structure

A broadside-coupled microstrip-to-CPW transition structure [19], [20] is adopted to feed the proposed inline CPW bandpass filter, as shown in Fig. 1. As a transition, this structure should provide a broadband transmission behavior. However, as a fed structure for the proposed CPW filter, it is only required to implement the predetermined capacitive coupling level. Therefore, the condition that the longitudinal coupled-strip length should approximately equal half-wavelength is no longer of necessity.

For spurious suppression, the broadside-coupled microstrip-to-CPW transition structure should properly be designed so as to provide required feeding capacitance ($C_{\rm feed}$) for the filter at the center frequency and to give a large insertion loss in the higher frequency band. Shown in Fig. 7 is the corresponding circuit layout fabricated on the 0.508-mm-thick RO4003 substrate for higher order spurious suppression and 1.5-GHz filter application. Here, the conductor and slot widths (W_2 and G_2) of the CPW portion are specified by the required impedance Z_2 for the SIR. The required metal–insulator–metal capacitance essentially determines the coupled-strip length D_f between the microstrip and CPW after assigning W_2

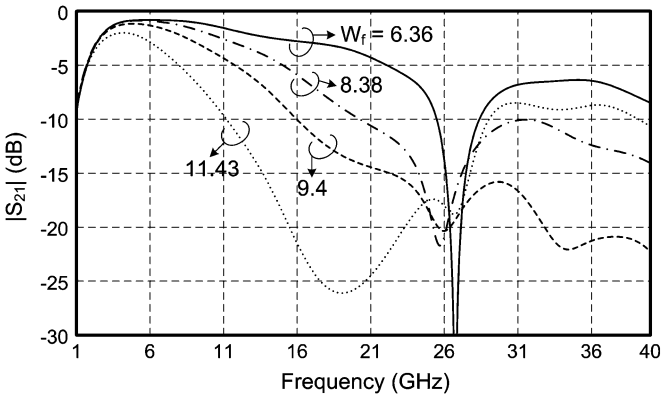

Fig. 8. Simulated frequency responses of the structure in Fig. 7 for various values of W_f. (Unit: millimeters).

($C_{\text{feed}} \approx \varepsilon_r \varepsilon_0 D_f W_2/h$). The remaining dimension left to be adjusted is W_f with $D_f = 1.1$ mm being fixed in characterizing this structure. Fig. 8 depicts the four sets of full-wave simulated frequency results under the selected dimensions for W_f.

When W_f just equals W_2, a deep transmission notch occurs at 26.64 GHz, which is the frequency at which W_f becomes a full-wavelength-long microstrip counterpart. Equivalently, the length measured from the open end of the upper microstrip to the feed-line center is equal to a half-wavelength. Physically, this notch may be associated with the fundamental resonance of a strip structure for which the oppositely directed vertical-coupled electric-field distributions between the overlapped portion of microstrip and CPW would be cancelled along the half-wavelength resonator; thus, no signal would pass through this transition. As W_f increases, the attenuation ability degrades gradually in the higher frequency band and the notch gets unobvious. Note that the response around 1.5 GHz remains unaltered, implying that the required capacitive coupling is almost unchanged as W_f is changed. Note that a critical value of 11.4 mm of W_f resulting in unfavorable rejection at high frequency over 25 GHz is observed in Fig. 8. In other words, W_f needs to be adjusted for our specification of the rejection band. In this demonstrated case, the optimal value of W_f for a high rejection level at high frequency ranges from 9.2 to 10.42 mm.

IV. Filter Design

For the proposed CPW filter with loaded air-bridge enhanced capacitors, its design procedure needs to be clearly specified. Based on the filter synthesis technique developed by Matthaei *et al.* [21], the general design equations for the proposed Nth-order filter, which is composed of $\lambda/4$ SIRs together with loaded capacitors, will systematically be established here.

Given the desired filter specification of center frequency (f_0) and factional bandwidth (Δ), Fig. 9 reveals the equivalent circuit of our proposed bandpass filter of order N loaded by lumped-element capacitors. The filter is made of $\lambda/4$ SIRs, which are coupled alternatively to J- and K-inverters. Each resonator is comprised of two joined transmission-line sections with impedances Z_1 and Z_2, and electrical lengths θ_1 and θ_2. The loaded capacitor for the resonator has a capacitance C_L. The equivalent circuits for the J- and K-inverter blocks shown in Fig. 9 are presented in Fig. 10(a) and (b). Defining $B_i(\omega) = \text{Im}[Y_{\text{ino}}(\omega)]$ and $X_i(\omega) = \text{Im}[Z_{\text{ins}}(\omega)]$ with Y_{ino} and Z_{ins} given by (1) and (2), the susceptance and reactance slope parameters can be obtained from their definitions as follows:

$$b_i = \frac{\omega_0}{2}\frac{\partial B_i(\omega)}{\partial \omega}\bigg|_{\omega_0} \qquad x_i = \frac{\omega_0}{2}\frac{\partial X_i(\omega)}{\partial \omega}\bigg|_{\omega_0}. \tag{6}$$

With the derived susceptance and reactance slope parameters, one may express the filter design parameters as

$$\begin{aligned} J_{01} &= \sqrt{\frac{\Delta \cdot Y_0 \cdot b_1}{g_0 \cdot g_1}} \\ K_{i,i+1} &= \sqrt{\frac{\Delta^2 \cdot x_i \cdot x_{i+1}}{g_i \cdot g_{i+1}}} \\ J_{i,i+1} &= \sqrt{\frac{\Delta^2 \cdot b_i \cdot b_{i+1}}{g_i \cdot g_{i+1}}} \\ J_{N,N+1} &= \sqrt{\frac{\Delta \cdot b_N \cdot Y_0}{g_N \cdot g_{N+1}}} \\ \theta'_{i,1} &= \theta_1 + \varphi_{i,i+1}/2 \\ \theta'_{i,2} &= \theta_2 + \varphi_{i,i+1}/2, \qquad i = 1, 2, \ldots, N-1 \end{aligned} \tag{7}$$

where g_i are the element values of the low-pass prototype filter. With the J- and K-inverter values calculated from (7), the corresponding capacitances, inductances, and electrical lengths may be found using the formulas for the conventional impedance and admittance inverters comprised of lumped and transmission-line elements [22]. As a result, the complete design formulas for the inline $\lambda/4$ bandpass filter with loaded capacitors are established.

In this study, the J-inverters at input and output stages will be implemented by the broadside-coupled microstrip-to-CPW transitions, as shown in Fig. 7, to provide suitable capacitive coupling at low frequency and spurious attenuation at high frequency. For the other J values, they are all realized by using the gap capacitors between the open ends of CPW SIRs, as shown in Fig. 11(a). The K-inverters are realized by the shunt inductors implemented between the short ends of CPW SIRs, as shown in Fig. 11(b). Note that the electrical length $\theta'_{i,1}$ and $\theta'_{i,2}$ may be converted to physical CPW lengths denoted as $D'_{i,1}$ and $D'_{i,2}$ through the propagation constants for different CPW impedances Z_1 and Z_2 of $\lambda/4$ resonators.

V. Mechanisms of WideBand Spurious-Suppression

A. Spurious Destruction

Very wide rejection band may potentially be achieved for the inline coplanar filter when appropriate spurious-suppression mechanisms are used. Based on the second-order filter with the equivalent circuit shown in Fig. 12, the concept for spurious destruction will qualitatively be discussed. At center frequency, the proposed filter (Fig. 12) is simply the cascade of two SIRs loaded by capacitors. On the foundation of the theory established by Matthaei *et al.* [21], an inline bandpass filter

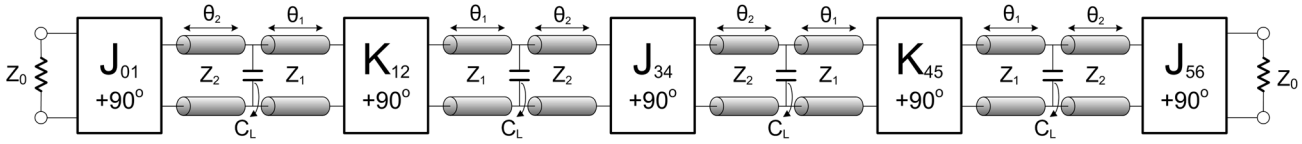

Fig. 9. Equivalent circuit of the proposed Nth-order bandpass filter using $\lambda/4$ SIRs with loaded lumped-element capacitors.

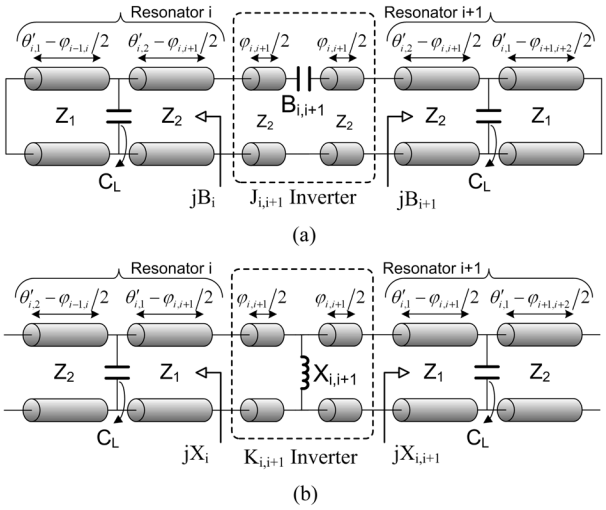

Fig. 10. (a) J-inverter network realized by series capacitor $C_{i,i+1}$. (b) K-inverter network realized by shunt inductor $L_{i,i+1}$ between resonators i and $(i+1)$.

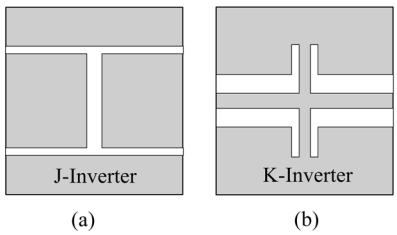

Fig. 11. Realizations of J- and K-inverters (capacitor and inductor) adopted in the proposed CPW filter. (White region: slot. Gray region: conductor.)

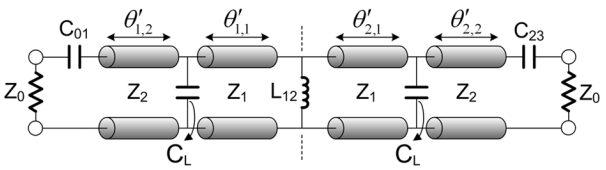

Fig. 12. Equivalent circuit of the proposed second-order bandpass filter with absence of odd-number spurious passbands.

using $\lambda/4$ TLs as its distributed elements requires J- and K-inverters placed alternatively between the resonant elements to produce a passband at a designated frequency. It implies that once the placement of J- and K-inverters does not follow the above-mentioned rule, the filter passband may be destructed. Instead of constructing the center passband, our proposed filter does exactly the opposite to destruct the spurious passband at $f_{\rm sp1}$. Our effort is to arrange an improper placement of J- and K-inverters at first spurious passband on the basis of the second-order filter. One can easily observe that there are four sections of

TABLE I
REQUIRED PARAMETERS FOR SECOND-ORDER BANDPASS FILTER SHOWN IN FIG. 12 WITH ABSENCE OF ODD-NUMBER SPURIOUS PASSBANDS

C_{01} (pF)	$\theta'_{1,2}$ (°)	$\theta'_{1,1}$ (°)	L_{12} (nH)	$\theta'_{2,1}$ (°)	$\theta'_{2,2}$ (°)	C_{23} (pF)
0.545	10.54	23.55	0.3545	23.55	10.54	0.545

TL in the second-order filter using capacitor-loaded SIRs. The two loaded capacitors C_L may be considered as another two K-inverters realized by shunt capacitors. By properly choosing the values of C_L, impedance ratio R_z, and length ratio u, the first spurious resonance $(f_{\rm sp1})$ can be pushed up to the frequency around $f_{\rm sp1} = k_{\rm sp1} f_0$. The frequency-dependent electrical lengths $\theta_1(f)$ and $\theta_2(f)$ at $f_{\rm sp1}$ will be $k_{\rm sp1}$ times their electrical lengths at f_0, i.e., $\theta_1(f_{\rm sp1}) = k_{\rm sp1}\theta_1(f_0), \theta_2(f_{\rm sp1}) = k_{\rm sp1}\theta_2(f_0)$, under the assumption that the electrical lengths are proportional to the frequency. Moreover, the capacitor-loaded SIR must appropriately be designed to give $k_{\rm sp1} \cdot \theta_1(f_0)$ and $k_{\rm sp1} \cdot \theta_2(f_0)$, which are simultaneously close to 90°. As a result, after the absorption of electrical lengths from J- and K-inverters at $f_{\rm sp1}$, the second-order filter configuration designed at f_0 behaves approximately like a cascade of J-90° TL-K-90° TL-K-90° TL-K-90° TL-J, equivalently a fourth-order filter with $\lambda/4$ resonators at $f_{\rm sp1}$. Since the J- and K-inverters are improperly arranged as expected, the spurious passband at $f_{\rm sp1}$ eventually will not appear.

A circuit-level simulation is conducted to demonstrate the spurious-destruction technique. To this end, a second-order filter is designed with center frequency $f_0 = 1.5$ GHz, and 3-dB fractional bandwidth of 10% for Chebyshev response. Choosing $C_L = 1.1$ pF, $u = 0.5, Z_1 = 111.8\ \Omega$, and $Z_2 = 54.95\ \Omega$, the corresponding electrical lengths of resonators will be $\theta_1 = \theta_2 = 25.26°$. The required design parameters for the second-order filter evaluated from (7) are listed in Table I. The calculated first five higher order spurious resonances are at 6.44, 11.07, 16.2, 21.57, and 26.45 GHz $(4.29f_0, 7.38f_0, 10.8f_0, 14.38f_0,$ and $17.63f_0)$, respectively, as shown in Fig. 13 (bottom half). Since the θ_1 and θ_2 at $f_{\rm sp1}$ are 108.4°, which would be close to 90° after the absorption of electrical lengths from the J- and K-inverters at $f_{\rm sp1}$, the condition for resonance destruction is met. The circuit simulation is carried out by AWR Microwave Office to get the frequency responses presented in Fig. 13 (upper half). Apparently, over the frequency range of 1.0–30 GHz, the filter only exhibits the spurious passbands around $f_{\rm sp2}$ $(7.38f_0)$ and $f_{\rm sp4}(14.38f_0)$, while the passbands at $f_{\rm sp1}(4.29f_0)$ and $f_{\rm sp3}(10.8f_0)$ are completely absent. In conclusion, the odd-number spurious resonances ($f_{\rm sp1}, f_{\rm sp3}$, etc.) will entirely be destructed due to the notion of improper inverter arrangement.

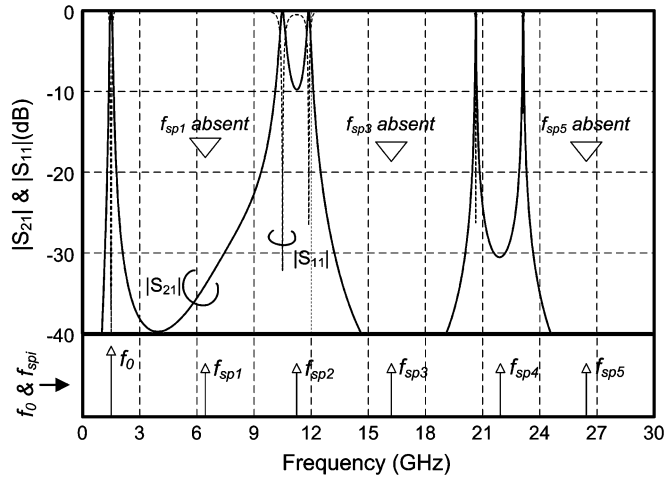

Fig. 13. Frequency responses of the proposed second-order filter (top half) described in Table I and the corresponding ith spurious (harmonic) frequencies denoted as $f_{\rm sp1}$ (bottom half).

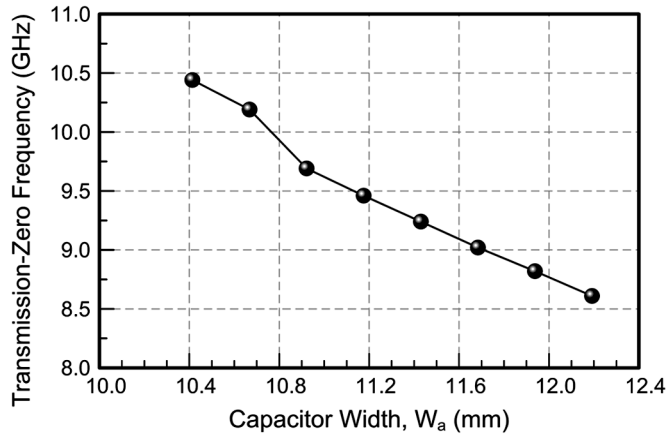

Fig. 14. Curve to relate transmission-zero frequencies, inherently associated with the air-bridge enhanced capacitor, to capacitor strip width W_a (Fig. 4).

B. Spurious Cancellation

A transmission zero is inherently created by the air-bridge enhanced capacitor structures discussed in Section II. Adjusting the dimensional sizes of strip, the transmission-zero position can be moved downward or upward to the specified frequency point. Based on the structure in Fig. 4 with all dimensions identical, except for W_a, the relation between the transmission-zero frequencies inherently associated with the air-bridge enhanced capacitor and the capacitor strip width W_a is plotted in Fig. 14. One can easily observe that the wider the strip, the lower the transmission-zero frequency. Intuitively, the related element values of the simplified model would be altered by adjusting the width W_a, but the C_s would only slightly be changed. To predict the generation of the transmission zero, the inductor presented in the simplified model for air-bridge enhanced capacitor needs to be included into the equivalent circuit of the proposed filter. Ensuring that the series resonance of the *LC* tank occurs exactly at $f_{\rm sp2}$, the spurious passband arising there will be suppressed. Once this spurious is cancelled, the next repeated passband for the demonstrated second-order filter listed in Table I will appear at 21.57 GHz $(14.38f_0)$.

C. Higher Order Spurious Attenuation

Thus far, three spurious passbands have been either destructed or suppressed with the innovative use of the air-bridge enhanced capacitors. The next effort is focused on the suppression of the rest of higher order resonances. The broadside-coupled microstrip-to-CPW transition described in Section III holds the possibility to attenuate the passed signal in the higher frequency band exceeding $14.38f_0$. As illustrated in Fig. 8, the microstrip-to-CPW transition structure resembles a low-pass structure when the dimensional sizes are optimally tuned. By designing the strip length W_f (Fig. 7) ranging from 9.2 to 10.42 mm, the higher order spurious passbands not lower than $14.38f_0$ may be attenuated. Of course, when fabricating this structure in a different substrate, this range might be different.

Eventually, the key steps to realize the proposed filter with a wide stopband are worthy of mention and are concluded as follows. First of all, the values of R_z and C_L should properly be chosen to make the utilized SIR with θ_1 and θ_2 approximately equal to 90° after the electrical-length absorption from inverters at the first spurious frequency $f_{\rm sp1}$ so that the odd-number spurious resonances $(f_{\rm sp1}, f_{\rm sp3}, \ldots)$ may entirely be destructed. The capacitor width W_a (Fig. 4) is then suitably adjusted such that the inherent transmission zeros associated with the air-bridge enhanced capacitor is allocated around $f_{\rm sp2}$, thereby canceling the second spurious passband around $f_{\rm sp2}$. Finally, the spurious passbands not lower than $f_{\rm sp4}$ is attenuated by optimally tuning the dimension W_f (Fig. 7) of the microstrip-to-CPW transition structures. By combining the above-mentioned spurious-suppression schemes, a very-wide rejection band can be accomplished in the proposed filter configuration.

VI. Filter Implementation and Results

Sufficient information for designing the inline CPW bandpass filters loaded by air-bridge enhanced capacitors with very-wide rejection bandwidth has been provided. To validate the design procedures, several filters based on the proposed structures are fabricated and thoughtfully examined.

A. Second-Order Filter

Spurious-destruction technique has been detailed qualitatively by simulating a second-order filter as an example in Section V. Further verification is done by fabricating the second-order filter with center frequency f_0 of 1.5 GHz, 3 dB-fractional bandwidth of 10% on the FR4 substrate ($\varepsilon_r = 4.3, h = 0.58$ mm, $\tan\delta = 0.02$). The SIRs possess the first four predicted spurious resonances at 6.69, 10.24, 16.7, and 19.77 GHz $(4.46f_0, 6.83f_0, 11.13f_0, 13.18f_0)$ with the given parameters $u = 0.47, R_z = 0.49, Z_1 = 111.8\ \Omega, Z_2 = 54.95\ \Omega$, and $C_L = 0.928$ pF. Accordingly, the corresponding electrical lengths of SIRs are $\theta_1 = 27.68°$ and $\theta_2 = 24.54°$. Since θ_1 and θ_2 at $f_{\rm sp1}$ are 123.45° and 109.45°, which are close to 90° after the electrical-length absorption from inverters, the resonance-destruction condition is met. The filter design parameters evaluated from (7) are listed in Table II. The air-bridge enhanced capacitor is designed with the extracted $L_s = 0.315$ nH and $C_s = 0.928$ pF to result in a transmission zero around 9.31 GHz for cancelling the spurious passbands at 9.56 GHz $(f_{\rm sp2})$. Note that the second spurious passband of the

TABLE II
REQUIRED PARAMETERS FOR FILTERS IN SECTION VI

Design	C_{01} (pF)	$\theta'_{1,2}$ (°)	$\theta'_{1,1}$ (°)	L_{12} (nH)	$\theta'_{2,1}$ (°)	$\theta'_{2,2}$ (°)	C_{23} (pF)
2nd-order C_L=0.93pF	0.52	10.37	25.8	0.384	25.8	10.37	0.52
4th-oder C_L=1.14pF	0.68	5.71	22.7	0.391	22.7	21.38	0.097

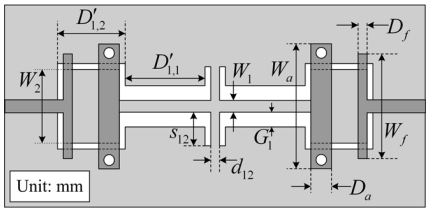

Fig. 15. Top-/bottom-plane layouts of the proposed second-order bandpass filter loaded by air-bridge enhanced capacitors described in Table II. ($W_1 = 1.02, G_1 = 1.27, W_2 = 6.35, G_2 = 0.51, D'_{1,2} = 5.9, D'_{1,1} = 6.93, s_{12} = 2.9, d_{12} = 0.76, W_a = 10.74, D_a = 1.78, D_f = 0.79, W_f = 9.02$).

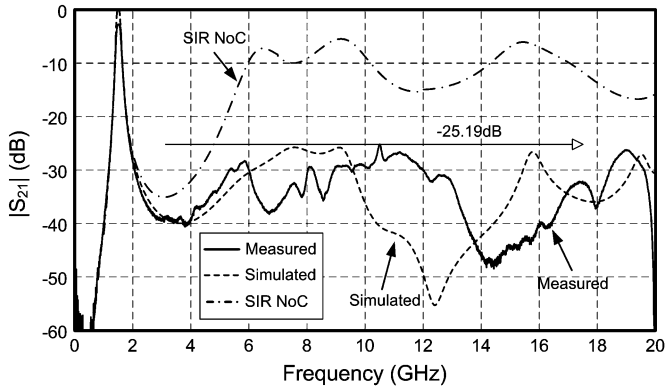

Fig. 16. Measured/simulated frequency responses of the proposed second-order filter fabricated on the 0.508-mm-thick FR4 substrate. (The second-order filter constructed by SIRs with identical R_z without loaded C_L is also included as "SIR-NoC" for comparison.)

fabricated filter shifts approximately 0.68 GHz lower than the calculated one. It is due to some parasitic effects of the CPW resonators using air-bridge enhanced capacitors not taken into consideration when calculating by (3). However, the resonance frequencies are still predicted accurately enough for our design. The physical layout is presented in Fig. 15 with dimensions labeled.

The full-wave simulated result with the dielectric loss excluded is shown in Fig. 16 together with the measured result for comparison. During the simulation, it is found that the loss obviously influences the in-band insertion loss, but is of minor significance on the out-of-band rejection. The fabricated filter has a center frequency at 1.549 GHz, measured 3-dB fractional bandwidth of approximately 11.27%, minimum insertion loss of 2.723 dB, and minimum passband return loss of 15.5 dB. The filter has a miniature size of only $0.18\lambda \times 0.07\lambda$, where λ stands for the wavelength of 50-Ω CPW at center frequency. This second-order bandpass filter possesses a stopband extended up to 20 GHz $(13.3f_0)$ with a rejection level better than 25.19 dB. No spurious passbands appear at 6.69 and 16.7 GHz because of spurious-destruction condition. The spurious resonance at 19.77 GHz $(13.18f_0)$ has also been effectively suppressed using the broadside-coupled microstrip-to-CPW transition structures. Note that the simulated result of the conventional inline CPW filter with identical $R_z = 0.49$ without loaded C_L is also presented in Fig. 16. It is found that the rejection level has been significantly improved in our proposed second-order filter.

B. Fourth-Order Filter

Intuitively, the attenuation level of the stopband can further be reinforced by increasing the filter order. Another fourth-order bandpass filter loaded by air-bridge enhanced capacitors is implemented on a 0.508-mm-thick RO4003 substrate. Since the fourth-order filter is symmetric with respect to C_{23} [see Fig. 17(a)], only the design parameters on the left-hand side of the equivalent circuit are presented in Table II. This filter is designed with $f_0 = 1.5$ GHz, 3-dB fractional bandwidth $= 10\%$ for the Chebyshev response. The equivalent circuit of this filter is illustrated in Fig. 17(a). Shown in Fig. 17(b) are the layouts of the fourth-order filter with dimensions labeled. The extracted L_s and C_s of the simplified equivalent model related to the dimensions of the air-bridge enhanced capacitor are 0.23 nH and 1.14 pF with respect to $W_a = 11.56$ mm and $D_a = 1.78$ mm. The $\lambda/4$ SIRs loaded by capacitors in this design have parameters, $u = 0.5, R_z = 0.5, Z_1 = 119.06\,\Omega, Z_2 = 60.02\,\Omega$, and $C_L = 1.14$ pF to satisfy the spurious-destruction condition. Accordingly, the predicted first four spurious resonances of utilized resonators are 6.58, 11.37, 16.85, and 22.22 GHz $(4.39f_0, 7.58f_0, 11.23f_0$, and $14.81f_0)$. The loaded air-bridge enhanced capacitors introduce an inherent transmission zero in the proximity of 9.83 GHz to cancel the second spurious passband at 9.92 GHz $(f_{\rm sp2})$. The offset of the second spurious passband is also due to the parasitic effects of the utilized SIRs not taken into consideration. The broadside-coupled microstrip-to-CPW transition has been optimally adjusted to possess $W_f = 1.12$ mm to increase the attenuation level exceeding 20 GHz.

Consequently, a very wide-stopband inline CPW filter has been fabricated. Its measured and simulated results are shown in Fig. 18. This fourth-order filter has a center frequency of 1.48 GHz, measured 3-dB fractional bandwidth of approximately 11.27%, minimum insertion loss of 1.73 dB, and minimum passband return loss of 15.5 dB. The proposed filter has a miniature size of only $0.42\lambda \times 0.07\lambda$. The stopband is extended up to 28.18 GHz $(19.04f_0)$ with a rejection level better than 30 dB. Note that the simulated results of a conventional inline CPW filter using $\lambda/4$ uniform-impedance resonators with the same specification is also included in Fig. 18 as a curve "Inline UIR" for reference. Remarkably, more than eight spurious passbands associated with the filter using a uniform-impedance resonator are suppressed in our proposed filter.

Note that there is some discrepancy between measured and simulated results from 5 to 13 GHz due to the inaccuracy of aligning the top- and bottom-plane layouts in the printed-circuit board fabrication. However, the level and trend of the measured out-of-band response are still predicted by the simulated one,

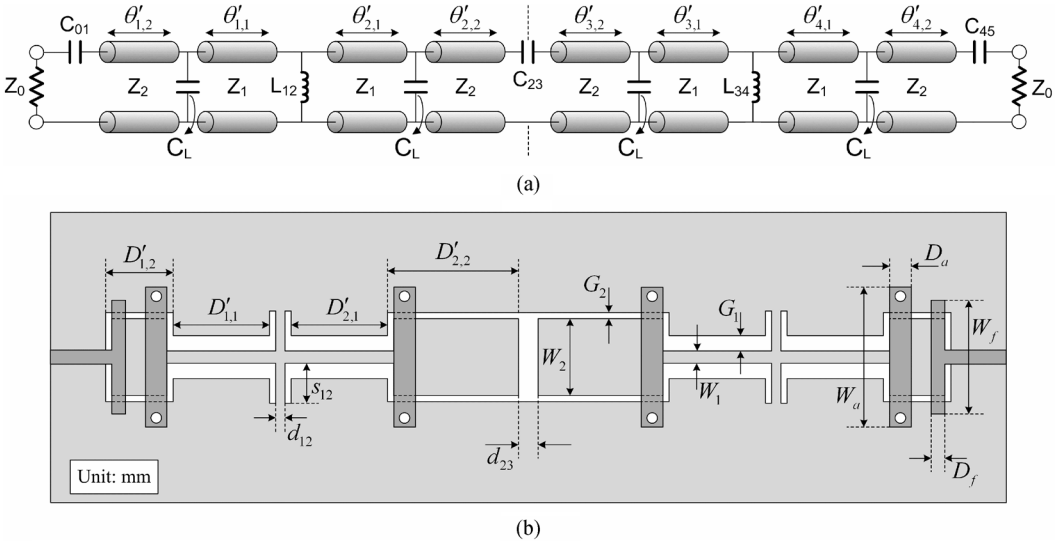

Fig. 17. (a) Equivalent circuit. (b) Top-/bottom-plane layouts of the proposed fourth-order CPW bandpass filter loaded by air-bridge enhanced capacitors described in Table II. ($W_1 = 1.02, G_1 = 1.27, W_2 = 6.35, G_2 = 0.51, D'_{1,2} = 5.05, D'_{1,1} = 7.95, s_{12} = 3.3, d_{12} = 0.76, D'_{2,1} = 7.95, D'_{2,2} = 10.8, d_{23} = 1.63, W_f = 1.12, D_f = 9.4, W_a = 11.56, D_a = 1.78$).

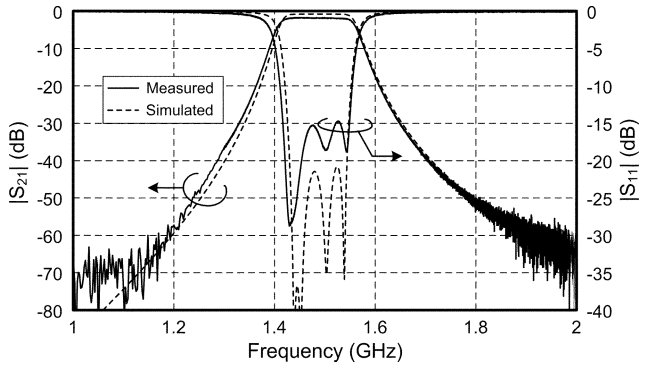

(a)

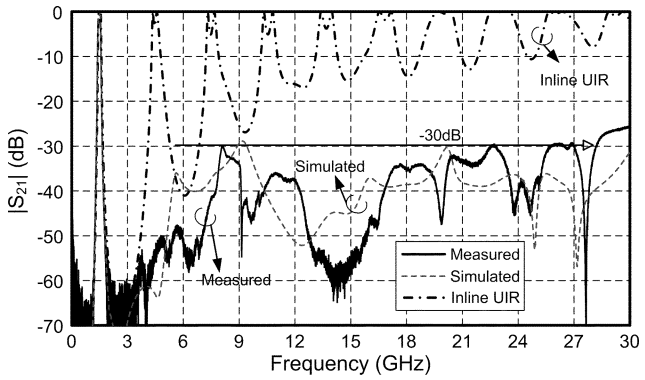

(b)

Fig. 18. (a) Narrowband and (b) wideband measured/simulated frequency responses of the proposed fourth-order filter described in Table II fabricated on the 0.508-mm-thick RO4003 substrate.

thereby verifying the three spurious suppression mechanisms, as mentioned in Section V.

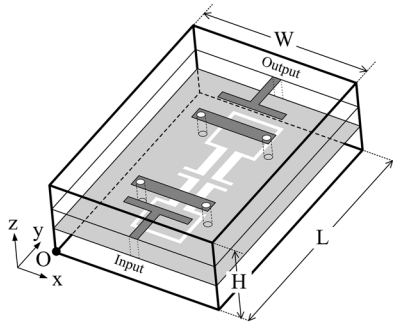

Fig. 19. Rectangular housing structure for the second-order filter in Fig. 15. ($W = 30.48$ mm, $L = 41.66$ mm, $H = 15.24$ mm). Note that the bold black lines represent the housing boundary and "O" indicates the coordinate origin.

VII. Housing Effects

For system application, the filter is usually surrounded by the metallic housing for preventing unnecessary interferences. Physically, the housing may cause unwanted cavity resonances to degrade the wideband spurious-suppression characteristic. It is very complicated to conduct the simultaneous design of the housing and filter. Therefore, a separate design of housing is essential from the practical point-of-view.

Note that the cavity resonances would eventually appear no matter how the housing is arranged and reshaped. An approach to effectively suppress the unwanted cavity resonances is to attach the absorbing material inside the housing walls.

Shown in Fig. 19 is a typical rectangular housing structure for the proposed second-order filter in Fig. 15. Curve 1 of Fig. 20 exhibits the simulated result of the filter with housing (but without the absorbing material). Obviously, the wideband spurious-suppression characteristic has been destructed due to the cavity resonances and the first spurious passband occurs at the resonant frequency of the cavity associated with the TE_{110} mode. By attaching the absorbing material on the top

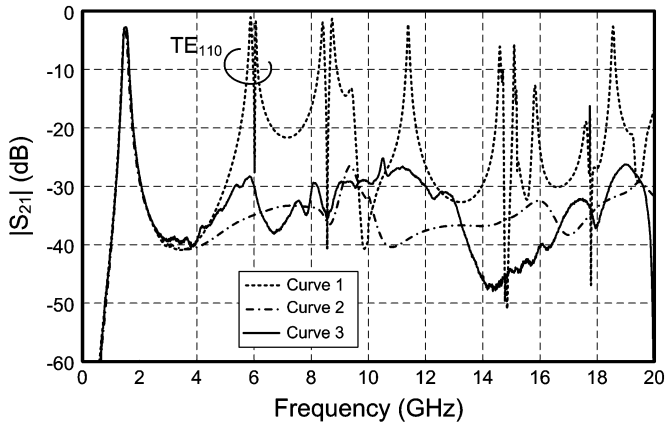

Fig. 20. Results of the second-order filter with and without the housing. (Curve 1: housing only, Curve 2: with absorber, Curve 3: without housing.)

and bottom walls of the housing, those unwanted resonances disappear, as shown in the simulated Curve 2 in Fig. 20. The ability of spurious suppression is recovered as well. Note that the measured result of the second-order filter (Curve 3) is also included in Fig. 20 for comparison.

VIII. Conclusion

To the authors' knowledge, the inline CPW bandpass filters loaded by capacitors with wideband spurious suppression have never been presented. The filters composed of $\lambda/4$ SIRs loaded by lumped-element capacitors with an absence of an odd number of spurious passbands are originally investigated in this study. Based on the mechanisms of the spurious destruction, the spurious cancellation due to the transmission zero inherently associated with the air-bridge enhanced capacitor structure, and the higher order spurious attenuation provided by broadside-coupled microstrip-to-CPW transition, the implemented fourth-order inline CPW filter has its stopband significantly extended up to $19.04f_0$ with a rejection level better than 30 dB. The implemented filter occupies a size also smaller than that of the conventional one due to the use of $\lambda/4$ resonators loaded by lumped-element capacitors. Since all occupied capacitors are realized in a dual-plane vertical configuration, the proposed inline CPW $\lambda/4$ filters are especially suitable for the multilayer fabrication process.

Acknowledgment

The authors would like to thank Dr. C.-H. Wang, National Taiwan University, Taipei, Taiwan, R.O.C., for his valuable discussions and suggestions on this topic.

References

[1] C. P. Wen, "Coplanar waveguide: A surface strip transmission line suitable for nonreciprocal gyromagnetic device applications," *IEEE Trans. Microw. Theory Tech.*, vol. MTT-17, no. 12, pp. 1087–1090, Dec. 1969.

[2] D. F. Williams and S. E. Schwarz, "Design and performance of coplanar waveguide bandpass filters," *IEEE Trans. Microw. Theory Tech.*, vol. MTT-31, no. 7, pp. 558–566, Jul. 1983.

[3] J. K. A. Everard and K. K. M. Cheng, "High performance direct coupled bandpass filters on coplanar waveguide," *IEEE Trans. Microw. Theory Tech.*, vol. 41, no. 9, pp. 1568–1573, Sep. 1993.

[4] A. Vogt and W. Jutzi, "An HTS narrow bandwidth coplanar shunt inductively coupled microwave bandpass filter on $LaAl_{03}$," *IEEE Trans. Appl. Supercond.*, vol. 45, no. 4, pp. 492–497, Apr. 1997.

[5] K. Wada and I. Awai, "Heuristic models of half-wavelength resonator bandpass filter with attenuation poles," *Electron. Lett.*, vol. 35, no. 5, pp. 401–402, Mar. 1999.

[6] H. Kanaya, J. Fujiyama, R. Oba, and K. Yoshida, "Design method of miniaturized HTS coplanar waveguide bandpass filters using cross coupling," *IEEE Trans. Appl. Supercond.*, vol. 13, no. 2, pp. 265–268, Jun. 2003.

[7] K. Wada, Y. Noguchi, E. Higashino, and J. Ishii, "Tapped-feed combline-type coplanar waveguide resonator bandpass filters," in *IEEE MTT-S Int. Microw. Symp. Dig.*, Feb. 1995, pp. 141–146.

[8] T. Tsujiguchi, H. Matsumoto, and T. Nishikawa, "A miniaturized end-coupled bandpass filter using $\lambda/4$ hair-pin coplanar resonators," in *IEEE MTT-S Int. Microw. Symp. Dig.*, Jun. 1998, pp. 829–832.

[9] M. Sagawa, M. Makimoto, and S. Yamashita, "Geometrical structures and fundamental characteristics of microwave stepped-impedance resonators," *IEEE Trans. Microw. Theory Tech.*, vol. 45, no. 7, pp. 1078–1085, Apr. 1997.

[10] A. Sanada, H. Takehara, and I. Awai, "Design of the CPW in-line $\lambda/4$ stepped-impedance resonator bandpass filter," in *Proc. Asia–Pacific Microw. Conf.*, Dec. 2001, pp. 633–636.

[11] J.-T. Kuo and E. Shih, "Microstrip stepped impedance resonator bandpass filter with an extended optimal rejection bandwidth," *IEEE Trans. Microw. Theory Tech.*, vol. 51, no. 5, pp. 1554–1559, May 2003.

[12] T. Lopetegi, M. A. G. Laso, J. Hernández, M. Bacaicoa, D. Benito, M. J. Garde, M. Sorolla, and M. Guglielmi, "New microstrip 'wiggly-line' filters with spurious passband suppression," *IEEE Trans. Microw. Theory Tech.*, vol. 49, no. 9, pp. 1593–1598, Sep. 2001.

[13] T. Lopetegi, M. A. G. Laso, F. Falcone, F. Martin, J. Bonache, J. Garcia, L. Perev-Cuevas, M. Sorolla, and M. Guglielmi, "Microstrip 'wiggly-line' bandpass filters with multispurious rejection," *IEEE Microwave Wireless Compon. Lett.*, vol. 14, no. 11, pp. 531–533, Nov. 2004.

[14] J.-T. Kuo, M. Jiang, and H.-J. Chang, "Design of parallel-coupled microstrip filters with suppression of spurious resonances using substrate suspension," *IEEE Trans. Microw. Theory Tech.*, vol. 52, no. 1, pp. 83–89, Jan. 2004.

[15] S.-C. Lin, P.-H. Den, Y.-S. Lin, C.-H. Wang, and C. H. Chen, "Wide-stopband microstrip bandpass filters using dissimilar quarter-wavelength stepped impedance resonators," *IEEE Trans. Microw. Theory Tech.*, vol. 54, no. 3, pp. 1011–1018, Mar. 2006.

[16] T. Tsujiguchi, H. Matsumoto, and T. Nishikawa, "A miniaturized double-surface CPW bandpass filter improved spurious responses," *IEEE Trans. Microw. Theory Tech.*, vol. 49, no. 5, pp. 879–885, May 2001.

[17] J. Gao and L. Zhu, "Asymmetric parallel-coupled CPW stages for harmonic suppressed $\lambda/4$ bandpass filters," *Electron. Lett.*, vol. 40, no. 18, pp. 1122–1123, Sep. 2004.

[18] C.-C. Chang, C. Caloz, and T. Itoh, "Analysis of a compact slot resonator in the ground plane for microstrip structures," in *Proc. Asia–Pacific Microw. Conf.*, Dec. 2001, pp. 1100–1103.

[19] J. J. Burke and R. W. Jackson, "Surface-to-surface transition via electromagnetic coupling of microstrip and coplanar waveguide," *IEEE Trans. Microw. Theory Tech.*, vol. 37, no. 3, pp. 519–525, Mar. 1989.

[20] L. Zhu and W. Menzel, "Broad-band microstrip-to-CPW transition via frequency-dependent electromagnetic coupling," *IEEE Trans. Microw. Theory Tech.*, vol. 52, no. 5, pp. 1517–1522, May 2004.

[21] G. Matthaei, L. Young, and E. Jones, *Microwave Filters, Impedance Matching Networks, and Coupling Structures*. New York: McGraw-Hill, 1964, pp. 427–440, 464–471.

[22] J. S. Hong and M. J. Lancaster, *Microstrip Filter for RF/Microwave Applications*. New York: Wiley, 2001, pp. 56–63.

Shih-Cheng Lin was born in Taitung, Taiwan, R.O.C., in 1981. He received the B.S. degree in electrical engineering from National Sun Yet-Sen University, Kaohsiung, Taiwan, R.O.C., in 2003, and is currently working toward the Ph.D. degree in communication engineering at National Taiwan University, Taipei, Taiwan, R.O.C.

His research interests include the design and analysis of microwave filter circuits and passive components.

Tsung-Nan Kuo was born in Taoyuan, Taiwan, R.O.C., in 1981. He received the B.S. degree in electrical engineering from National Dong Hwa University, Hualien, Taiwan, R.O.C., in 2003, the M.S.E.E. degree from National Taiwan University, Taipei, Taiwan, R.O.C., in 2005, and is currently working toward the Ph.D. degree at National Taiwan University.

His research interests include the design and analysis of microwave filter circuits.

Yo-Shen Lin (M'04) was born in Taipei, Taiwan, R.O.C. in 1973. He received the B.S. and M.S.E.E. degrees in electrical engineering and Ph.D. degree in communication engineering from National Taiwan University, Taipei, Taiwan, R.O.C., in 1996, 1998, and 2003, respectively.

From 1998 to 2001, he was an RF Engineer with the Acer Communication and Multimedia Inc., Taipei, Taiwan, R.O.C., where he designed global system for mobile communication (GSM) mobile phones. From 2001 to 2003, he was with the Chi-Mei Communication System Inc., Taipei, Taiwan, R.O.C., where he was involved with the design of low-temperature co-fired ceramic (LTCC) RF transceiver modules for GSM mobile applications. In August 2003, he joined the Graduate Institute of Communication Engineering, National Taiwan University, as a Post-Doctoral Research Fellow, and became an Assistant Professor in August 2004. Since August 2005, he has been with the Department of Electrical Engineering, National Central University, Chungli, Taiwan, R.O.C., where he is currently an Assistant Professor. His research interests include the design and analysis of miniature planar microwave circuits and RF transceiver module for wireless communication systems.

Dr. Lin was the recipient of the Best Paper Award presented at the 2001 Asia–Pacific Microwave Conference (APMC), Taipei, Taiwan, R.O.C. and the 2005 Young Scientist Award presented at the URSI General Assembly, New Delhi, India.

Chun Hsiung Chen (SM'88–F'96) was born in Taipei, Taiwan, R.O.C., on March 7, 1937. He received the B.S.E.E. and Ph.D. degrees in electrical engineering from National Taiwan University, Taipei, Taiwan, R.O.C., in 1960 and 1972, respectively, and the M.S.E.E. degree from National Chiao Tung University, Hsinchu, Taiwan, R.O.C., in 1962.

In 1963, he joined the Faculty of the Department of Electrical Engineering, National Taiwan University, where he is currently a Professor. From August 1982 to July 1985, he was Chairman of the Department of Electrical Engineering, National Taiwan University. From August 1992 to July 1996, he was the Director of the University Computer Center, National Taiwan University. In 1974, he was a Visiting Scholar with the Department of Electrical Engineering and Computer Sciences, University of California at Berkeley. From August 1986 to July 1987, he was a Visiting Professor with the Department of Electrical Engineering, University of Houston, Houston, TX. In 1989, 1990, and 1994, he visited the Microwave Department, Technical University of Munich, Munich, Germany, the Laboratoire d'Optique Electromagnetique, Faculte des Sciences et Techniques de Saint-Jerome, Universite d'Aix-Marseille III, Marseille, France, and the Department of Electrical Engineering, Michigan State University, East Lansing, respectively. His areas of interest include microwave circuits and computational electromagnetics.